MAJOR ARTICLE

Noninvasive Molecular Imaging of Tuberculosis-Associated Inflammation With Radioiodinated DPA-713

Catherine A. Foss,[1,2,a] Jamie S. Harper,[1,3,a] Haofan Wang,[2] Martin G. Pomper,[1,2] and Sanjay K. Jain[1,3]

[1]Center for Infection and Inflammation Imaging Research, [2]Russell H. Morgan Department of Radiology and Radiological Science, and [3]Department of Pediatrics, Johns Hopkins University School of Medicine, Baltimore, Maryland

Background. Increased expression of translocator protein (TSPO) is a feature of microglial and macrophage activation. Since activated macrophages are key components of tuberculosis-associated inflammation, we evaluated radioiodinated DPA-713, a synthetic ligand of TSPO, for in vivo imaging of host response.

Methods. Mice were infected with aerosolized *Mycobacterium tuberculosis* and evaluated using whole-body [^{125}I]iodo-DPA-713 single-photon emission computed tomography (SPECT). Ex vivo biodistribution and correlative immunofluorescence studies were also performed.

Results. [^{125}I]Iodo-DPA-713 SPECT imaging clearly delineated tuberculosis-associated pulmonary inflammation in live animals. Biodistribution studies confirmed radiotracer specificity for inflamed pulmonary tissues. Immunofluorescence studies demonstrated that TSPO is highly expressed in CD68^{+} macrophages and phagocytic cells within tuberculosis lesions and that [^{125}I]DPA-713 specifically accumulates within these cells. Coadministration of excess unlabelled DPA-713 abrogated both the SPECT and ex vivo fluorescence signals. Lesion-specific signal-to-noise ratios were significantly higher with [^{125}I]iodo-DPA-713 SPECT (4.06 ± 0.52) versus [^{18}F]fluorodeoxyglucose (FDG) positron emission tomography (PET) (2.00 ± 0.28) performed in the same mice ($P = .004$).

Conclusions. [^{125}I]Iodo-DPA-713 accumulates specifically in tuberculosis-associated inflammatory lesions by selective retention within macrophages and phagocytic cells. [^{125}I]Iodo-DPA-713 SPECT provides higher lesion-specific signal-to-noise ratios than [^{18}F]FDG PET and may prove to be a more specific biomarker to monitor tuberculosis in situ.

Keywords. translocator protein; molecular imaging; tuberculosis; PET; pyrazolopyrimidine; macrophage.

Compared with other technologies, imaging can evaluate disease processes deep within the host (or organ) noninvasively and relatively rapidly. Other major advantages of imaging include the ability to provide a 3-dimensional assessment of the whole organ or body, enabling a complete view of the disease process in relevant tissues and the ability to conduct noninvasive longitudinal assessments in the same individual. While continued advances in molecular imaging have provide unparalleled opportunities for more refined methods to monitor diseases in the field of oncology [1], tools for evaluating infection remain limited. This is clearly evident with the current methods used to monitor tuberculosis. Sputum cultures, which have remained the standard for monitoring tuberculosis treatments, are limited because sputum bacterial burdens are not available in real time (4–6 weeks delay for results). Even though new tests based on nucleic acid amplification (NAA) may be able to provide results more rapidly [2], both culture and NAA are subject to sampling bias because they only assess lesions communicating with the airways. Since *Mycobacterium tuberculosis* can infect virtually any part of the lung (including extrapulmonary

Received 25 January 2013; accepted 7 March 2013; electronically published 30 July 2013.

[a]C. A. F. and J. S. H. contributed equally to this work.

Presented in part: Symposium on Molecular Imaging of Infectious Diseases: Current Status and Future Challenges, Bethesda, Maryland, 21 September 2012.

Correspondence: Sanjay K. Jain, MD, Center for Infection and Inflammation Imaging Research, Johns Hopkins University School of Medicine, 1550 Orleans St, CRB-II, Rm 1.09, Baltimore, MD 21287 (sjain5@jhmi.edu).

The Journal of Infectious Diseases 2013;208:2067–74

DOI: 10.1093/infdis/jit331

sites), these methods do not always correlate closely with overall disease. For the same reasons, imaging can also elucidate important findings with regard to the pathophysiology of tuberculosis, which are difficult, if not impossible, to assess with the current technologies.

Optical imaging techniques have been used for noninvasive imaging of several bacterial infections, including tuberculosis [3–8]. While optical imaging has excellent sensitivity, detection is limited by the depth of the signal. Therefore, this technology is usually limited to use in small animals. Imaging technologies such as computed tomography (CT) and [^{18}F]fluorodeoxyglucose (FDG) positron emission tomography (PET) are not limited by the location and depth of the signal and are therefore being increasingly used to detect and monitor infections [9–11] and for assessment of tuberculosis treatments [12, 13] in both preclinical and clinical settings. However, the major limitation of standard CT and [^{18}F]FDG PET is a lack of specificity, with [^{18}F]FDG uptake by several different types of metabolically active cells [14–16]. Since activated macrophages are key components of tuberculosis-associated inflammation, macrophage-avid tracers could serve as more specific imaging agents to monitor the *M. tuberculosis*–host interactions.

Translocator protein (TSPO) is an 18-kDa trans-mitochondrial membrane channel for transport of cholesterol and other endogenous ligands [17]. TSPO expression is highest in steroidogenic tissues, heart, lung, and kidney, as well as in immune cells, such as activated microglia and macrophages [18]. We and others have used TSPO as a molecular target for imaging neuroinflammation [17, 19, 20]. Recently, a variety of TSPO-specific radioligands have also been used to detect inflammation in peripheral tissues, such as in atherosclerotic plaque [21], breast tumors [22], bone [23], and lungs [24, 25]. In this study, we evaluated radioiodo-DPA-713, a low-molecular-weight pyrazolopyrimidine ligand for TSPO, as an imaging biomarker for pulmonary tuberculosis–associated inflammation in mouse models of tuberculosis [26, 27]. Noninvasive imaging with [^{125}I]iodo-DPA-713 single-photon emission computed tomography (SPECT) and high-resolution CT were performed to detect tuberculosis lesions in live animals. Ex vivo immunofluorescence studies were also performed to evaluate the specificity and cellular localization of DPA-713 in tuberculosis lesions.

MATERIALS AND METHODS

All protocols were approved by the Johns Hopkins Biosafety, Radiation Safety, and Animal Care and Use Committees.

Animal Infection

Female BALB/c (Charles River Labs, Frederick, MD) or C3HeB/FeJ (Jackson Laboratory, Bar Harbor, ME) mice aged 4–8 weeks were infected with aerosolized *M. tuberculosis* H37Rv, using the Middlebrook Inhalation Exposure System (Glas-Col, Terre Haute, IN), with frozen titrated bacterial stocks. At least 4 mice (for each strain and time point) were used to determine the bacillary burden 1 day after infection and at the time of analyses [12, 27]. A total of 20 mg/kg of unlabelled DPA-713 (to effect auto-blockade of TSPO) [28] was co-administered to additional uninfected animals and infected animals, which served as controls.

Imaging

Live animals were imaged within sealed biocontainment devices [12, 29]. Each mouse was weighed and injected intravenously (in the tail vein) with 37 MBq (500 pmol) of [^{125}I]iodo-DPA-713 [25] and imaged 24 hours after injection with the NanoSPECT/CT (Bioscan, Washington, DC) imager, using 24 projections at 100 seconds per projection (60-minute static scan). Four mice were used for each group and mouse strain (except for the infected, unblocked C3HeB/FeJ group, which had only 3 mice). Infected C3HeB/FeJ mice also underwent [^{18}F]FDG PET as described previously [12]. All images were reconstructed and coregistered with CT images, using either Amide, version 0.9.1 (available at: http://amide.sourceforge.net), or Amira, version 5.2.2 (Visage Imaging, San Diego, CA), and standardized uptake values (SUV) computed as described previously [12]. By use of the coregistered CT images as a reference, spherical (diameter, 1.5 mm) regions of interest (ROIs) were traced around the same regions and applied to the SPECT and PET data. Lesion-specific signal-to-noise ratios were calculated by dividing the mean activity in tuberculosis lesions by the mean activity in controls (uninfected lung) for each animal.

Biodistribution Studies

Mice were intravenously injected with 85 kBq (1.15 pmol) of [^{125}I]iodo-DPA-713 and euthanized 24 hours after injection. Organs were harvested, individually weighed, and disinfected with 10% formalin. The radioactivity for each organ was measured using an automated gamma counter (1282 Compugamma, LKB Wallac, Mt. Waverly, Australia). Five mice were used for each group and mouse strain.

Immunofluorescence Studies

Lung tissues were harvested after systemic perfusion with phosphate-buffered saline under deep anesthesia, fixed with 10% formalin, sectioned, and probed with primary and fluorescent secondary antibodies (Supplementary Table 1). Slides were viewed using a Nikon 80i epifluorescence microscope (Melville, NY). Lung tissues from an additional set of mice intravenously injected with 8 pmol of DPA-713-IRDye680LT, a fluorescent analog of DPA-713, were collected as described above following euthanization 24 hours after injection.

Statistical Analysis

Comparisons for biodistribution studies were performed using a 1-tailed Mann-Whitney *U* test (available at: http://elegans.

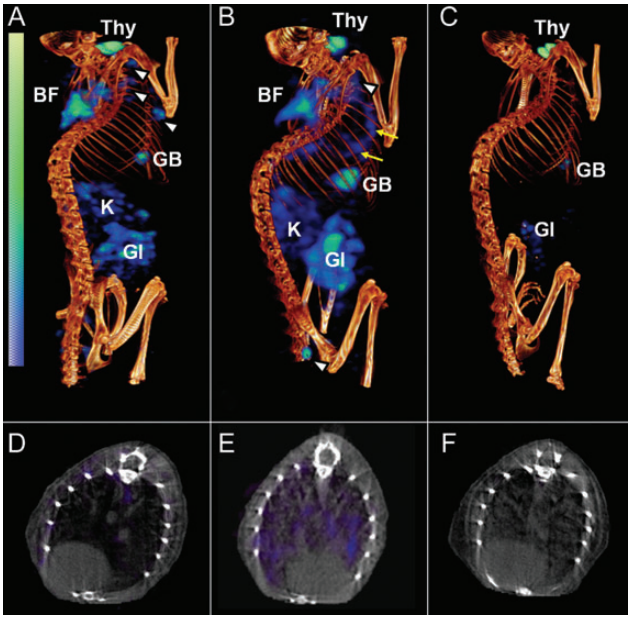

Figure 1. [^{125}I]Iodo-DPA-713 single-photon emission computed tomography–high-resolution CT (SPECT-CT) of BALB/c mice. Coregistered [^{125}I]iodo-DPA-713 SPECT-CT images from representative *Mycobacterium tuberculosis*–infected BALB/c mice are shown. Compared with uninfected control mice (*A* and *D*), in which only a minimal pulmonary SPECT signal is noted, significant but diffuse signal is observed in the lungs of infected mice (*B* and *E*, yellow arrows). Auto-blockade abrogates the SPECT signal from the lungs of infected mice (*C* and *F*). Signal is also noted in brown fat (BF), lymph nodes (white arrowheads), gastrointestinal tract (GI), kidneys/adrenal glands (K), gallbladder (GB), and thyroid (Thy).

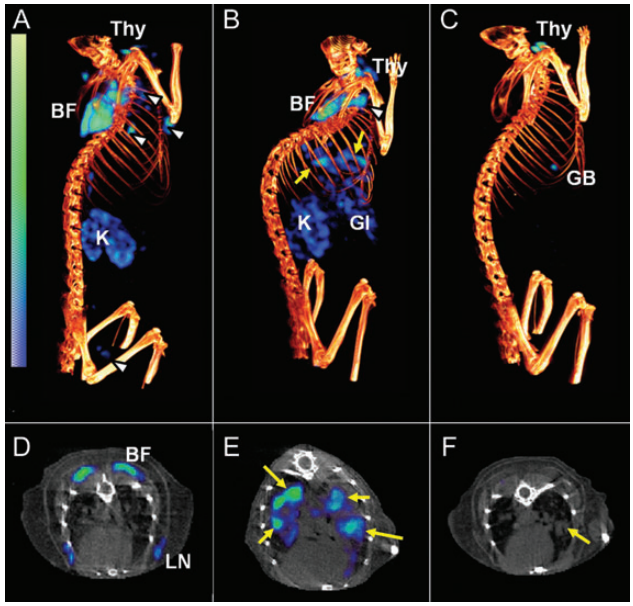

Figure 2. [^{125}I]Iodo-DPA-713 single-photon emission computed tomography–high-resolution CT (SPECT-CT) of C3HeB/FeJ mice. Coregistered [^{125}I]iodo-DPA-713 SPECT-CT images from representative *Mycobacterium tuberculosis*–infected C3HeB/FeJ mice are shown. Compared with uninfected control mice (*A* and *D*), in which only minimal pulmonary SPECT signal is noted, discrete areas of signal, colocalizing with the tuberculosis lesions seen on CT, are observed in the infected mouse (*B* and *E*, yellow arrows). Auto-blockade abrogates the SPECT signal from the lungs of infected-mice (*C*). While the tuberculosis lesion is clearly seen on the CT image (*F*, yellow arrow), no corresponding SPECT signal is noted because of the auto-blockade. Signal is also noted in brown fat (BF), lymph nodes (white arrowheads), gallbladder (GB), thyroid (Thy), lymph node (LN), gastrointestinal tract (GI), and kidneys/adrenal glands (K).

som.vcu.edu/~leon/stats/utest.html). Comparisons for quantitative imaging data were performed using a 1-tailed distribution, 2-sample unequal variance Student *t* test in Excel 2007 (Microsoft). Data are presented on a linear scale, except for colony-forming units (CFU), for which a logarithmic scale (mean ± SD) is used.

RESULTS

We evaluated [^{125}I]iodo-DPA-713, a synthetic ligand for TSPO, as an imaging agent for tuberculosis-associated pulmonary inflammation. To simulate human disease, we infected C3HeB/FeJ mice with low-dose aerosolized *M. tuberculosis* and allowed the infection to incubate for 6–8 weeks to allow pulmonary lesions to evolve into well-formed discrete necrotic, hypoxic lesions akin to those in infected humans [26, 27]. We infected BALB/c mice with a higher-dose of aerosolized *M. tuberculosis* to achieve a bacterial growth plateau 2–3 weeks after infection. Pulmonary implantations of *M. tuberculosis* 1 day after aerosol infection for BALB/c and C3HeB/FeJ mice were 4.59 ± 0.08 and 1.11 ± 0.13 $\log_{10}$ CFU, respectively.

Imaging

Pulmonary bacterial burdens at the time of imaging for BALB/c mice (2 weeks after infection) and C3HeB/FeJ mice (8 weeks after infection) were 9.37 ± 0.07 and 6.89 ± 0.43 $\log_{10}$ CFU, respectively. Representative volume-rendered [^{125}I]iodo-DPA-713 SPECT-CT images (scaled to the injected dose) are shown in Figure 1 (BALB/c mice) and Figure 2 (C3HeB/FeJ mice). SPECT signal (blue) is clearly noted in the lungs of the infected mice (Figure 1*B* and Figure 2*B*), with little to no signal in the lungs of the uninfected animals (Figure 1*A* and Figure 2*A*) or animals in which blocking occurred (Figure 1*C* and Figure 2*C*). Discrete areas of SPECT signal (Figure 2*B* and 2*E*), corresponding to the necrotic tuberculosis lesions in the lungs of the infected C3HeB/FeJ mice, is also clearly noted. All mice displayed some uptake in the gallbladder and thyroid, whereas uninfected and infected mice in panels A and B showed gut and kidney/adrenal uptake, which was blocked by coadministration of DPA-713, indicating that all peripheral uptake aside from that in the gallbladder and thyroid was specific. Thyroid uptake is due to metabolic radiodehalogenation and organification of

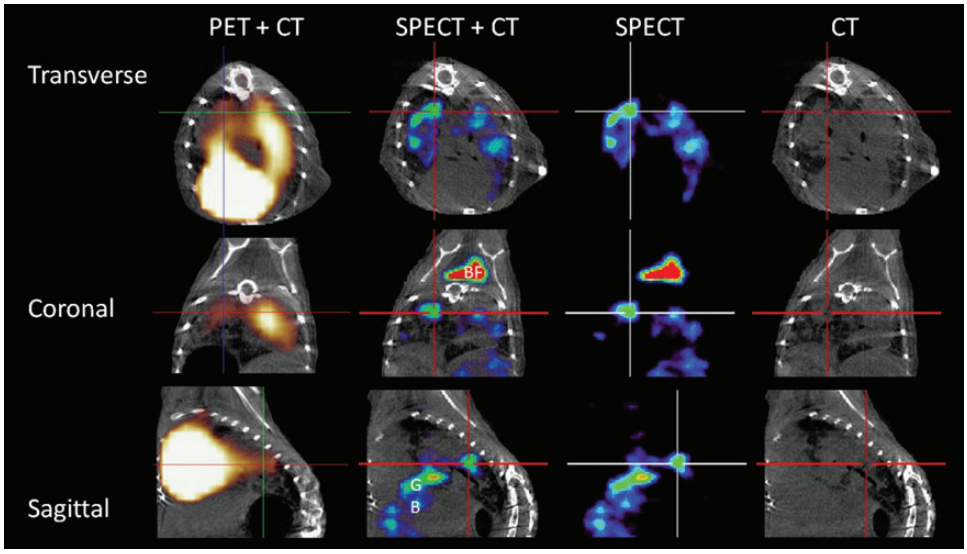

Figure 3. [^{125}I]Iodo-DPA-713 localizes to tuberculosis lesions. The transverse, coronal, and sagittal images from a representative *Mycobacterium tuberculosis*–infected C3HeB/FeJ mouse that underwent both [^{125}I]iodo-DPA-713 single-photon emission computed tomography–high-resolution CT (SPECT-CT) and [^{18}F]FDG positron emission tomography (PET)–high-resolution CT are shown. Discrete areas of [^{125}I]iodo-DPA-713 SPECT signal are noted in the lungs of the infected mouse. The SPECT signal colocalizes with the tuberculosis lesion seen on CT (crosshair). The [^{18}F]FDG PET signal is more diffuse, with intense signal noted in the heart, obscuring the pericardiac regions. [^{125}I]iodo-DPA-713 SPECT signal is also noted in the brown fat (BF) in the coronal view.

free [^{125}I] [30], whereas adrenal glands and kidneys (in the cortex) express TSPO [31].

Figure 3 shows a direct comparison of [^{125}I]iodo-DPA-713 SPECT and [^{18}F]FDG PET images of the same animal. While a discrete [^{125}I]iodo-DPA-713 SPECT signal is noted only at the sites of tuberculosis lesions, the [^{18}F]FDG PET signal is more diffuse. In addition, an intense [^{18}F]FDG PET signal is also noted in the heart and liver, which is nonspecific for inflammation, obscures the adjacent pulmonary regions, and makes monitoring of specific lesions more difficult. Lesion-specific signal-to-noise ratios (±SD) were significantly higher with [^{125}I]iodo-DPA-713 SPECT (4.06 ± 0.52) than with [^{18}F]FDG PET (2.00 ± 0.28) performed on the same mice ($P = .004$). These data indicate that after 24 hours of radiotracer uptake, [^{125}I]iodo-DPA-713 accumulates specifically within pulmonary tuberculosis–associated lesions in infected mice and provides higher signal-to-noise ratios than [^{18}F]FDG PET.

Biodistribution

Mean pulmonary bacterial burdens (±SD) at the time of analyses for BALB/c mice (2 weeks after infection) and C3HeB/FeJ mice (6 weeks after infection) were 7.89 ± 0.06 and 7.00 ± 0.11 $\log_{10}$ CFU, respectively. The tissue accumulations of [^{125}I]iodo-DPA-713 after 24 hours of uptake are shown in Table 1. Since the liver expresses comparatively low levels of TSPO [32] and represents the best approximation of target-to-nontarget tissue near the tissue of interest, SUV comparisons were made between the lung and liver tissues. This ratio serves as an important normalization, allowing for accurate dose-independent comparison of longitudinal measurements. Of all tissues sampled, only the infected lungs demonstrated a significantly higher retention of tracer. Lung-to-liver ratios were significantly higher in infected BALB/c mice, compared with uninfected BALB/c mice (7.55 vs 3.86; $P = .014$). Auto-blockade of TSPO significantly decreased this ratio in infected mice (2.38; $P = .029$). Similarly, lung-to-liver ratios were also significantly higher in infected C3HeB/FeJ mice versus uninfected C3HeB/FeJ mice (8.38 vs 4.95; $P = .014$), with auto-blockade of TSPO decreasing this ratio in infected mice (2.75; $P = .001$), confirming the radiotracer specificity for pulmonary tissues.

TSPO Expression in Tuberculosis Granulomas

M. tuberculosis is known to inhabit densely accumulated peripheral macrophages that surround the necrotic cores of granulomas in humans [33]. We therefore performed immunofluorescence studies on lung sections from BALB/c or C3HeB/FeJ mice to delineate the cellular expression of TSPO. Sections focusing on the pneumonic tissues (BALB/c) or the cellular margin of the tuberculosis granuloma (C3HeB/FeJ) are shown in Figure 4. This region is rich in activated macrophages, and TSPO is expressed at high levels. Close inspection of stained macrophages reveals what appears to be substantial colocalization of TSPO and CD68 staining on both the plasma membrane and perinuclear region (Figure 5). Collectively, these data demonstrate that TSPO is highly expressed in macrophages in tuberculosis-associated inflammatory lesions.

Table 1. Tissue Biodistribution of [^{125}I]iodo-DPA-713

	BALB/c Mice, SUV, Median (Range)			C3HeB/FeJ Mice, SUV, Median (Range)		
Organ(s)	Uninfected	Infected	Infected (Auto-Blockade)	Uninfected	Infected	Infected (Auto-Blockade)
Lung:liver	5.01 (4.60–6.00)	6.04 (5.56–6.99)	2.46 (1.81–2.82)	4.94 (4.52–6.25)	8.38 (5.68–14.22)	2.75 (1.12–4.57)
Lung[a]:liver	3.86 (3.34–4.29)	7.55 (5.39–8.33)	2.38 (0.32–3.48)	. . .	. . .	. . .
Lung	0.90 (0.83–1.08)	1.01 (0.93–1.17)	0.11 (0.00–0.12)	0.49 (0.45–0.50)	0.71 (0.48–1.20)	0.12 (0.00–0.21)
Lung[a]	0.70 (0.60–0.77)	1.26 (0.90–1.39)	0.10 (0.01–0.15)	. . .	. . .	
Liver	0.18 (0.16–0.22)	0.17 (0.16–0.17)	0.04 (0.04–0.06)	0.10 (0.08–0.10)	0.08 (0.07–0.11)	0.05 (0.03–0.06)
Blood	0.02 (0.02–0.03)	0.02 (0.01–0.02)	0.01 (0.00–0.04)	0.01 (0.00–0.01)	0.01 (0.01–0.01)	0.01 (0.00–0.02)
Heart	0.55 (0.40–0.65)	0.48 (0.47–0.51)	0.04 (0.02–0.05)	0.25 (0.24–0.26)	0.19 (0.14–0.24)	0.04 (0.02–0.05)
Stomach	0.69 (0.64–0.81)	0.66 (0.60–0.73)	0.09 (0.06–0.09)	0.38 (0.20–0.25)	0.21 (0.19–0.33)	0.04 (0.05–0.22)
Pancreas	0.40 (0.34–0.44)	0.40 (0.35–0.44)	0.03 (0.02–0.04)	0.24 (0.48–0.54)	0.18 (0.16–0.23)	0.03 (0.02–0.04)
Spleen	0.96 (0.83–1.04)	0.95 (0.84–1.02)	0.09 (0.08–0.11)	0.54 (0.76–0.95)	0.44 (0.31–0.50)	0.06 (0.04–0.08)
Kidney	1.68 (1.37–1.86)	1.58 (1.51–1.66)	0.15 (0.11–0.16)	0.94 (0.27–0.36)	0.76 (0.66–0.93)	0.10 (0.06–0.13)
Brown fat	1.47 (1.05–1.59)	1.02 (0.95–1.33)	0.26 (0.20–0.31)	0.35 (0.39–0.52)	0.41 (0.19–0.54)	0.10 (0.04–0.13)
Small intestine	0.66 (0.50–0.80)	0.71 (0.65–0.97)	0.08 (0.06–0.18)	0.40 (0.48–0.67)	0.41 (0.30–0.46)	0.05 (0.03–0.12)
Large intestine	0.99 (0.89–1.12)	1.09 (1.09–1.14)	0.24 (0.15–0.37)	0.54 (0.14–0.17)	0.39 (0.37–0.47)	0.18 (0.09–0.28)
Muscle	0.41 (0.24–0.53)	0.39 (0.35–0.41)	0.02 (0.02–0.03)	0.17 (0.19–0.23)	0.11 (0.09–0.14)	0.01 (0.01–0.02)
Bladder	0.33 (0.31–0.36)	0.21 (0.16–0.28)	0.13 (0.11–0.17)	0.21 (0.07–0.12)	0.16 (0.11–0.21)	0.08 (0.04–0.16)
Bone	0.28 (0.25–0.31)	0.24 (0.19–0.27)	0.02 (0.00–0.02)	0.09 (0.13–0.27)	0.07 (0.06–0.09)	0.01 (0.01–0.03)
Ovary	0.46 (0.43–0.52)	0.42 (0.29–0.57)	0.09 (0.05–0.10)	0.23 (0.01–0.01)	0.19 (0.09–0.27)	0.07 (0.05–0.10)
Brain	0.02 (0.02–0.02)	0.02 (0.01–0.02)	0.00 (0.00–0.00)	0.01 (0.01–0.01)	0.01 (0.01–0.01)	0.00 (0.00–0.00)

Standardized uptake values (SUVs) were calculated for all tissues as the percentage of injected dose per gram of tissue per body weight.

[a] SUV data are calculated as the percentage of injected dose per organ per body weight for uninfected BALB/c mice, to correct for pulmonary edema noted in the infected BALB/c mice.

DPA-713 Colocalizes With Macrophages and Phagocytic Cells Within Tuberculosis Lesions

To determine cellular uptake and specificity, lung tissues from infected C3HeB/FeJ mice and infected but TSPO–auto-blockaded mice were probed following intravenous administration of fluorescent analog of DPA-713 (DPA-713-IRDye680LT; Figure 6). While signal from ex vivo DPA-713-IRDye680LT is clearly noted in the lung tissues from the infected mouse (Figure 6*B*), which colocalizes with the CD68 signal (Figure 6*E*), no DPA-713-IRDye680LT signal is noted in the mouse with auto-blockaded TSPO. These data demonstrate specific retention of DPA-713 by macrophages and phagocytic cells within tuberculosis lesions.

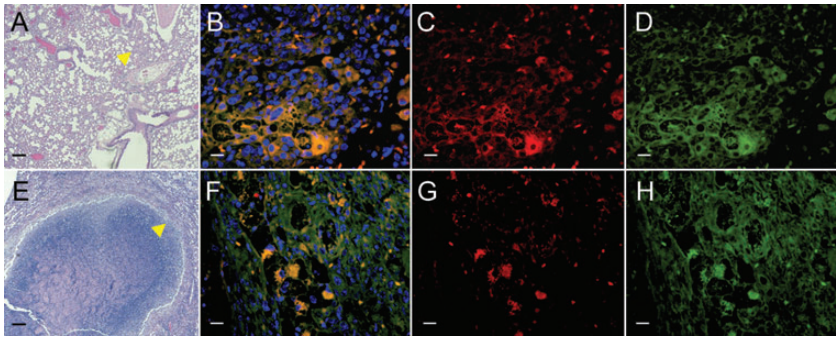

Figure 4. Translocator protein (TSPO) expression in tuberculosis lesions. Lung sections from *Mycobacterium tuberculosis*–infected BALB/c mice or C3HeB/FeJ mice show pneumonic tissues (BALB/c; *A* [arrow]) or the cellular margins of a necrotic tuberculosis granuloma (C3HeB/FeJ; *E* [arrow]). This region has dense infiltration by inflammatory cells, such as lymphocytes and activated macrophages. Higher-power views (*A* and *E*; yellow arrows) demonstrate immunostaining for TSPO (*C* and *G*; red), CD68 (*D* and *H*; green), and overlay of TSPO and CD68 with nuclear stain (*B* and *F*) are also shown. Note that there are many CD68^{+} cells in this region, with high TSPO expression that colocalizes with the CD68 signal (yellow; *B* and *F*). Scale bars represent 100 μm (for *A* and *E*) or 25 μm (for all other panels).

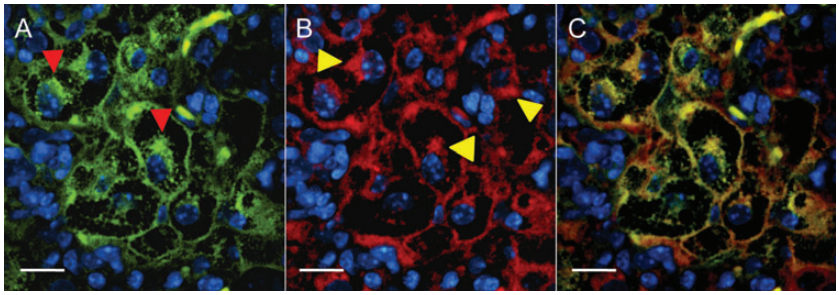

Figure 5. Subcellular translocator protein (TSPO) expression in macrophages within tuberculosis lesions. A magnified view of a cluster of macrophages from the cellular margin of a tuberculosis granuloma show the CD68 signal (*A*; red arrowheads) from the macrophages. *B*, Corresponding TSPO expression with perinuclear and plasma membrane localization (yellow arrowheads). *C*, (overlay of *A* and *B*) demonstrates that the TSPO expression colocalizes substantially with the CD68 signal within the cells. Scale bars represent 25 μm.

DISCUSSION

Tuberculosis remains one of the leading causes of morbidity and mortality worldwide [34]. While there have been recent efforts in developing better control measures, tools used to monitor tuberculosis continue to have significant limitations. Inappropriate and incomplete treatments increase the risk for developing drug resistance and have contributed to multidrug resistant–, extensively drug resistant, and totally drug resistant tuberculosis [35, 36]. Accordingly, there is significant interest in developing validated biomarkers to monitor tuberculosis, both in the research and clinical settings [37]. Efficient, noninvasive and species-independent biomarkers could be used to monitor disease and could expedite translation of new tuberculosis drugs and vaccines.

Our overall goal was to evaluate [^{125}I]iodo-DPA-713 as an in vivo imaging agent for tuberculosis-associated inflammation. We have demonstrated that [^{125}I]iodo-DPA-713 localizes within tuberculosis lesions in infected lungs of both the mouse models used in this study. Moreover, coadministration of excess DPA-713 abrogated the SPECT signal, demonstrating that uptake and retention of [^{125}I]iodo-DPA-713 is due to specific binding. Since [^{18}F]FDG PET is being increasingly used to detect and monitor tuberculosis [12, 13], we also directly compared [^{125}I]iodo-DPA-713 SPECT and [^{18}F]FDG PET imaging in the same mice. While discrete signals colocalizing with the tuberculosis lesion were readily apparent with [^{125}I]iodo-DPA-713 SPECT, corresponding [^{18}F]FDG PET displayed poor contrast between tuberculosis lesions and normal lung tissues. The intense [^{18}F]FDG signal from the myocardium and liver also partially obscured the surrounding lung tissues. Moreover, lesion-specific signal-to-noise ratios were significantly higher with [^{125}I]iodo-DPA-713 SPECT and suggest that [^{125}I]iodo-DPA-713 may prove to be a more specific method to detect and monitor tuberculosis-associated inflammation in vivo. To corroborate the imaging findings, ex vivo biodistribution studies

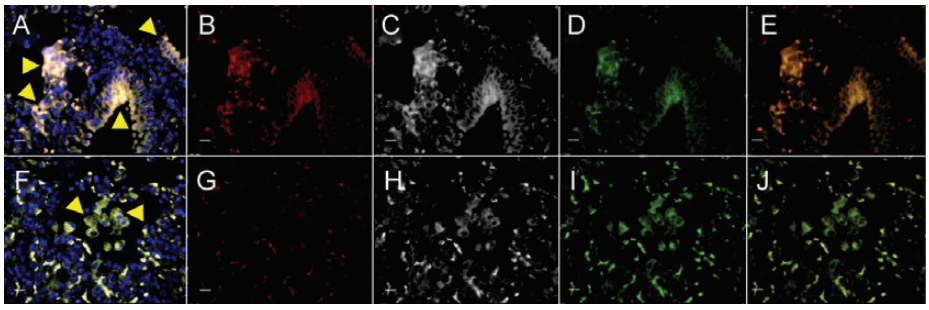

Figure 6. DPA-713 accumulates within macrophages. Lungs from infected C3HeB/FeJ mice (*A*–*E*) and infected but translocator protein (TSPO)–auto-blockaded mice (*F*–*J*) were harvested and processed 24 hours following intravenous administration of DPA-713-IRDye680LT (fluorescent analog of DPA-713). Signal from DPA-713-IRDye680LT (*B* and *G*; red), TSPO (*C* and *H*; white), CD68 (*D* and *I*; green), overlay of CD68 with DPA-713-IRDye680LT (*E* and *J*), and overlay of all channels with nuclear stain (*A* and *F*) are shown. DPA-713-IRDye680LT signal is clearly noted in lung tissues obtained from the infected mouse (*B*; red) and colocalizes with CD68 (*E*; yellow). However, while both TSPO (*H*) and CD68 (*I*) signals are visible in the lung tissues from the infected but TSPO–auto-blockaded mouse, no DPA-713-IRDye680LT signal is noted (*G*). Arrows point to a cluster of macrophages or CD68^{+} phagocytic cells. Scale bars represent 25 μm.

were also performed. The uptake of [^{125}I]iodo-DPA-713 in lung tissues was significantly higher in infected mice, compared with uninfected mice, and blocking decreased this uptake significantly. It should be noted that unlike imaging studies, in which lesion-specific measurements are made by tracing ROIs around the infected-lung tissues, biodistribution studies measure [^{125}I]iodo-DPA-713 uptake for the whole organ, which comprises both diseased and nondiseased tissues. This considerably reduces the apparent pulmonary uptake by averaging focal lesion uptake with the surrounding, nondiseased, low-uptake pulmonary tissues. However, we have demonstrated that high contrast and resolution between tuberculosis lesions and normal tissues is both achievable and measurable with imaging studies.

We also evaluated TSPO expression in the tuberculosis granulomas, using immunofluorescence. Our data demonstrate that TSPO is expressed in macrophages and other CD68$^+$ phagocytic cells within tuberculosis lesions. Substantial colocalization of TSPO and CD68 may also suggest a putative lysosomal location for TSPO alongside lysosomal CD68. This would juxtapose cholesterol-bound oxidized low-density lipoprotein binding by CD68 [38] with cholesterol binding by TSPO [21]. Since TSPO is endogenously expressed in bronchoalveolar epithelial cells [39], we also probed lung sections to delineate TSPO distribution in other cells. TSPO expression (colocalizing with CD68$^+$ cells) was also noted within the airway (Supplementary Figure 1), suggesting that iodo-DPA-713 is selectively retained not only in macrophages, but also other CD68$^+$ phagocytic cells within infected lung tissues. Finally, to evaluate whether macrophages associated with tuberculosis granulomas were the cellular target for [^{125}I]iodo-DPA-713, we performed ex vivo studies with DPA-713-IRDye680LT (a fluorescent analog of DPA-713) to correlate the imaging findings at a microscopic level. Tuberculosis granulomas from chronically infected mice demonstrated colocalization of ex vivo DPA-713-IRDye680LT signal with CD68$^+$ and TSPO-positive macrophages. This signal could be abrogated by coinjection of DPA-713, indicating that macrophages are the targets for selective retention of DPA-713 after 24 hours of radiotracer distribution.

Typically, radiolabeled DPA-713 analogs, including [^{11}C]DPA-713 and [^{125}I]iodo-DPA-713, have been assessed at relatively early time points, ≤90 minutes of distribution [19, 25, 28, 40, 41]. We evaluated both the typical 1-hour time point and subsequent uptake times and determined that a 24-hour uptake period was optimal and yielded a favorable in vivo retention of [^{125}I]iodo-DPA-713 (Supplementary Figure 2). The longer physical half-life of radioiodine species permits observance of this 24-hour distribution and selective retention period and allows inflammatory pulmonary lung lesions to be easily discerned, even within the background of TSPO-positive lung tissues. Though it is established that TSPO is the target for DPA-713, additional (TSPO-like) targets, present only in phagocytic (and related cell types), may also be selectively trapping DPA-713, as has been demonstrated by others by use of different TSPO ligands [42].

In summary, these studies demonstrate specific accumulation of [^{125}I]iodo-DPA-713 within tuberculosis-associated pulmonary lesions. [^{125}I]Iodo-DPA-713 imaging provides higher lesion-specific signal-to-noise ratios than does [^{18}F]FDG PET imaging in mice and may prove to be a more specific method to detect and monitor tuberculosis-associated inflammation in vivo. Real-time, serial observational capabilities of radioiodo-DPA-713 imaging may augment the study of mycobacterial pathogenesis and monitoring of disease in real time. Since iodo-DPA-713 can be labeled with either direct γ (I-123) or positron-emitting (I-124) radioisotopes, all with biologically appropriate half-lives, radioiodinated DPA-713 has the potential to be a useful SPECT or PET probe for clinical applications involving tuberculosis-associated inflammatory biology. Radioiodo-DPA-713 imaging could be easily translated to clinical settings, such as tuberculosis trials, where resources are not as limited but where rapid and accurate biomarkers for monitoring tuberculosis treatments and relapse are urgently required. In addition, since imaging provides immediate readouts, they may also permit the use of adaptive designs for clinical trials, which will provide significant and additional cost savings. Finally, radioiodo-DPA-713 imaging will also be useful for several other macrophage-associated pulmonary infectious or inflammatory conditions, such as fungal infections and sarcoidosis.

Supplementary Data

Supplementary materials are available at *The Journal of Infectious Diseases* online (http://jid.oxfordjournals.org/). Supplementary materials consist of data provided by the author that are published to benefit the reader. The posted materials are not copyedited. The contents of all supplementary data are the sole responsibility of the authors. Questions or messages regarding errors should be addressed to the author.

Notes

Acknowledgment. We thank Mariah Klunk at the Center for Infection and Inflammation Imaging Research, Johns Hopkins University, for her assistance in biodistribution studies.

Disclaimer. The funders had no role in study design, data collection and analysis, decision to publish, or preparation of the manuscript.

Financial support. This work was supported by the National Institutes of Health (Director's New Innovator Award OD006492 to S. K. J., HL116316-01 to S. K. J., and grant EB009367 to M. G. P.).

Potential conflict of interest. All authors: No reported conflicts.

All authors have submitted the ICMJE Form for Disclosure of Potential Conflicts of Interest. Conflicts that the editors consider relevant to the content of the manuscript have been disclosed.

References

1. Higgins LJ, Pomper MG. The evolution of imaging in cancer: current state and future challenges. Semin Oncol **2011**; 38:3–15.

2. Boehme CC, Nabeta P, Hillemann D, et al. Rapid molecular detection of tuberculosis and rifampin resistance. N Engl J Med **2010**; 363:1005–15.
3. Zelmer A, Carroll P, Andreu N, et al. A new in vivo model to test anti-tuberculosis drugs using fluorescence imaging. J Antimicrob Chemother **2012**; 67:1948–60.
4. Andreu N, Zelmer A, Wiles S. Noninvasive biophotonic imaging for studies of infectious disease. FEMS Microbiol Rev **2011**; 35:360–94.
5. Kong Y, Yao H, Ren H, et al. Imaging tuberculosis with endogenous beta-lactamase reporter enzyme fluorescence in live mice. Proc Natl Acad Sci U S A **2010**; 107:12239–44.
6. Ning X, Lee S, Wang Z, et al. Maltodextrin-based imaging probes detect bacteria in vivo with high sensitivity and specificity. Nat Mater **2011**; 10:602–7.
7. Clay H, Volkman HE, Ramakrishnan L. Tumor necrosis factor signaling mediates resistance to mycobacteria by inhibiting bacterial growth and macrophage death. Immunity **2008**; 29:283–94.
8. Egen JG, Rothfuchs AG, Feng CG, Winter N, Sher A, Germain RN. Macrophage and T cell dynamics during the development and disintegration of mycobacterial granulomas. Immunity **2008**; 28: 271–84.
9. Kei PL, Kok TY, Padhy AK, Ng DC, Goh AS. [18F] FDG PET/CT in patients with fever of unknown origin: a local experience. Nucl Med Commun **2010**; 31:788–92.
10. Keidar Z, Gurman-Balbir A, Gaitini D, Israel O. Fever of unknown origin: the role of 18F-FDG PET/CT. J Nucl Med **2008**; 49:1980–5.
11. Meller J, Sahlmann CO, Scheel AK. 18F-FDG PET and PET/CT in fever of unknown origin. J Nucl Med **2007**; 48:35–45.
12. Davis SL, Nuermberger EL, Um PK, et al. Noninvasive pulmonary [18F]-2-fluoro-deoxy-D-glucose positron emission tomography correlates with bactericidal activity of tuberculosis drug treatment. Antimicrob Agents Chemother **2009**; 53:4879–84.
13. Sathekge M, Maes A, Kgomo M, Stoltz A, Van de Wiele C. Use of 18F-FDG PET to predict response to first-line tuberculostatics in HIV-associated tuberculosis. J Nucl Med **2011**; 52:880–5.
14. Bell GI, Burant CF, Takeda J, Gould GW. Structure and function of mammalian facilitative sugar transporters. J Biol Chem **1993**; 268:19161–4.
15. Pauwels EK, Ribeiro MJ, Stoot JH, McCready VR, Bourguignon M, Maziere B. FDG accumulation and tumor biology. Nucl Med Biol **1998**; 25:317–22.
16. Zhuang H, Alavi A. 18-fluorodeoxyglucose positron emission tomographic imaging in the detection and monitoring of infection and inflammation. Semin Nucl Med **2002**; 32:47–59.
17. Rupprecht R, Papadopoulos V, Rammes G, et al. Translocator protein (18 kDa) (TSPO) as a therapeutic target for neurological and psychiatric disorders. Nat Rev Drug Discov **2010**; 9:971–88.
18. Zavala F, Haumont J, Lenfant M. Interaction of benzodiazepines with mouse macrophages. Eur J Pharmacol **1984**; 106:561–6.
19. Endres CJ, Pomper MG, James M, et al. Initial evaluation of 11C-DPA-713, a novel TSPO PET ligand, in humans. J Nucl Med **2009**; 50:1276–82.
20. Fujimura Y, Zoghbi SS, Simeon FG, et al. Quantification of translocator protein (18 kDa) in the human brain with PET and a novel radioligand, (18)F-PBR06. J Nucl Med **2009**; 50:1047–53.
21. Bird JL, Izquierdo-Garcia D, Davies JR, et al. Evaluation of translocator protein quantification as a tool for characterising macrophage burden in human carotid atherosclerosis. Atherosclerosis **2010**; 210: 388–91.
22. Zheng J, Boisgard R, Siquier-Pernet K, Decaudin D, Dolle F, Tavitian B. Differential expression of the 18 kDa translocator protein (TSPO) by neoplastic and inflammatory cells in mouse tumors of breast cancer. Mol Pharm **2011**; 8:823–32.
23. Kam WW, Meikle SR, Dunstan CR, Banati RB. The 18 kDa translocator protein (peripheral benzodiazepine receptor) expression in the bone of normal, osteoprotegerin or low calcium diet treated mice. PLoS One **2012**; 7:e30623.
24. Hatori A, Yui J, Yamasaki T, et al. PET imaging of lung inflammation with [(18)F]FEDAC, a radioligand for translocator protein (18 kDa). PLoS One **2012**; 7:e45065.
25. Wang H, Pullambhatla M, Guilarte TR, Mease RC, Pomper MG. Synthesis of [(125)I]iodoDPA-713: a new probe for imaging inflammation. Biochem Biophys Res Commun **2009**; 389:80–3.
26. Pan H, Yan BS, Rojas M, et al. Ipr1 gene mediates innate immunity to tuberculosis. Nature **2005**; 434:767–72.
27. Harper J, Skerry C, Davis SL, et al. Mouse model of necrotic tuberculosis granulomas develops hypoxic lesions. J Infect Dis **2012**; 205: 595–602.
28. Doorduin J, Klein HC, Dierckx RA, James M, Kassiou M, de Vries EF. [11C]-DPA-713 and [18F]-DPA-714 as new PET tracers for TSPO: a comparison with [11C]-(R)-PK11195 in a rat model of herpes encephalitis. Mol Imaging Biol **2009**; 11:386–98.
29. Davis SL, Be NA, Lamichhane G, et al. Bacterial thymidine kinase as a non-invasive imaging reporter for Mycobacterium tuberculosis in live animals. PLoS One **2009**; 4:e6297.
30. Savoie JC, Thomopoulos P, Savoie F. Studies on mono- and diiodohistidine. I. The identification of iodohistidines from thyroidal iodoproteins and their peripheral metabolism in the normal man and rat. J Clin Invest **1973**; 52:106–15.
31. Favreau F, Rossard L, Zhang K, et al. Expression and modulation of translocator protein and its partners by hypoxia reoxygenation or ischemia and reperfusion in porcine renal models. Am J Physiol Renal Physiol **2009**; 297:F177–90.
32. Batarseh A, Papadopoulos V. Regulation of translocator protein 18 kDa (TSPO) expression in health and disease states. Mol Cell Endocrinol **2010**; 327:1–12.
33. Fenton MJ, Vermeulen MW. Immunopathology of tuberculosis: roles of macrophages and monocytes. Infect Immun **1996**; 64:683–90.
34. WHO. Global tuberculosis control: WHO report. Geneva: Global Tuberculosis Programme, World Health Organization, **2012**.
35. Emergence of Mycobacterium tuberculosis with extensive resistance to second-line drugs–worldwide, 2000–2004. MMWR Morb Mortal Wkly Rep **2006**; 55:301–5.
36. Velayati AA, Masjedi MR, Farnia P, et al. Emergence of new forms of totally drug-resistant tuberculosis bacilli: super extensively drug-resistant tuberculosis or totally drug-resistant strains in iran. Chest **2009**; 136:420–5.
37. Schluger NW. Tuberculosis clinical trials: past, present and future. Presented at: Keystone Symposia. Tuberculosis: from lab research to field trials, Vancouver, Canada. March 20–25, 2007.
38. Ramprasad MP, Terpstra V, Kondratenko N, Quehenberger O, Steinberg D. Cell surface expression of mouse macrosialin and human CD68 and their role as macrophage receptors for oxidized low density lipoprotein. Proc Natl Acad Sci U S A **1996**; 93:14833–8.
39. Hardwick MJ, Chen MK, Baidoo K, Pomper MG, Guilarte TR. In vivo imaging of peripheral benzodiazepine receptors in mouse lungs: a biomarker of inflammation. Mol Imaging **2005**; 4:432–8.
40. Boutin H, Chauveau F, Thominiaux C, et al. 11C-DPA-713: a novel peripheral benzodiazepine receptor PET ligand for in vivo imaging of neuroinflammation. J Nucl Med **2007**; 48:573–81.
41. Endres CJ, Coughlin JM, Gage KL, Watkins CC, Kassiou M, Pomper MG. Radiation Dosimetry and Biodistribution of the TSPO Ligand 11C-DPA-713 in Humans. J Nucl Med **2012**; 53:330–5.
42. Sexton M, Woodruff G, Cudaback E, et al. Binding of NIR-conPK and NIR-6 T to astrocytomas and microglial cells: evidence for a protein related to TSPO. PLoS One **2009**; 4:e8271.